An experimental study on the heat transfer performance of a prototype molten-salt rod baffle heat exchanger for concentrated solar power

Yu Qiu, Ya-Ling He, Wen-Qi Wang, Bao-Cun Du, Kun Wang

Turbulent convective heat transfer of molten salt in the shell side of a prototype rod baffle heat exchanger for concentrating solar power

Yu Qiu, Ya-Ling He*, Wen-Qi Wang, Bao-Cun Du, Kun Wang

Key Laboratory of Thermo-Fluid Science and Engineering of Ministry of Education , School of Energy and Power Engineering, Xi'an Jiaotong University, Xi'an, Shaanxi 710049, China

Abstract: In this paper, a prototype rod baffle shell-and-tube heat exchanger (RB-STHX) was designed and fabricated for concentrating solar power (CSP). In order to investigate the heat transfer characteristics of molten salt in the shell side, the RB-STHX was experimentally studied. A ternary salt Hitec and an oil were adopted as the heat transfer fluids in the shell and tube sides, respectively. Experimental data was firstly obtained with the salt temperature of 212.7~279.6^{o}C, where the corresponding Prandtl number is in the range of 14.2~23.3. The flow is in the turbulent region with the Reynolds number of 2,697 to 12,517. The average heat transfer rate ranges from 117 kW to 364 kW. Then, the experimental data were compared with two exiting correlations. The results indicate that an average error of -9.1 ~ -12.3% between the Nusselt numbers predicted by the two exiting correlations and the experiment data was found. Finally, for predicting the heat transfer characteristics of the molten salt in the shell side more accurately, two modified heat transfer correlations which show satisfactory agreements with the experimental data were developed. The average deviation between the experiment data and the modified correlations are around ±4.4 ~ ±4.6%. Results from present study will offer the reliable experimental data, useful correlations and helpful guidance for the design and operation of realistic molten salt RB-STHXs in the CSP systems.

Keywords: Molten salt; Rod baffle shell-and-tube heat exchanger; Shell-side heat transfer characteristics; Experimental study; Concentrating solar power

1. Introduction

* Corresponding author.

The fossil fuel combustion has leaded to serious environmental issues and public health risks for years[1-4]. The Concentrating Solar Power (CSP) technology which generates electricity from concentrated solar radiation has been regarded as a candidate for solving these problems[5, 6]. As a result, the CSP has developed quickly in the last few decades. In CSP plants, the thermal energy storage[7, 8], which usually uses molten salt as energy storage material and allows energy dispatch, is widely adopted. In the thermal storage unit, shell-and-tube heat exchangers (STHXs) are used to exchange thermal energy between this unit and the rest of the plant[9]. For the middle temperature thermal storage in linear Fresnel reflector[10, 11] and parabolic trough collector[12, 13], both the Salt-Water/Steam STHXs and the Salt-Oil STHXs are employed. While for high temperature thermal storage in solar power tower[14], only the Salt-Water/Steam STHXs are adopted. In the Salt-Oil STHXs, the salt usually flows in the shell side. In Salt-Water/Steam STHXs, the salt usually flows in the shell sides of salt-water preheater, evaporator and superheater. In a few designs, the salt also flows in the tube side of the salt-water evaporator.

It is well known that the convective heat transfer characteristics (CHTCs) of molten salt in both tube and shell sides of the STHXs directly influence the performance of the thermal storage unit. As a result, they are important for the design and operation of the plants. For these reasons, many experimental studies have focused on investigating the CHTCs of molten salt.

Review of the literature from 1940s to 2017, it is found that most experiments are conducted for studying on the CHTCs in circular tubes. Many of these studies are conducted using different salts under uniform flux. Grele and Gedeon[15] studied the CHTCs of FLiNaK with Pr=1.23-4.33 and Re=2000-20,000. Hoffman[16] also studied the CHTCs of FLiNaK with Pr=1.6-4 and Re=2428-9,536. He also studied the CHTCs of a ternary nitrate salt Hitec with Pr=3.3-9.1 and Re=2342-33,493[17]. Cooke and Cox[18] studied the CHTCs of LiF-BeF2-ThF4-UF4 with Pr=4-14 and Re=400~30,600. Silverman et al.[19] studied the CHTCs of LiF-BeF2-ThF2-UF4 with Pr=6.6-14.2 and Re=1,542-14,210, and they also studied the CHTCs of NaBF4-NaF with Pr=4.89-5.64 and Re=5,104-44,965. Moreover, some

of these studies are conducted using salts in the tube side of a concentric tube heat exchanger (HX). Wu et al.[20, 21] used $LiNO_3$ with *Pr*=12.7-14.7, *Re*=17,000-45,000. They also used Hitec with *Pr*=8.1-23.9, *Re*=3184-34,861. Chen et al.[22] used another ternary nitrate salt with *Re*=10000-50000 and *Pr*=11-27. In addition, it is also found that several studies have investigated the CHTCs of molten salt in the tube side of STHXs. He et al.[23] studied the CHTCs of Hitec in the tube-side of the tube bundle in a Salt-Oil STHX with *Re*=9,000-19,000 and *Pr*=6.5-10. Jin et al.[24] studied the CHTCs in the tube side of a Salt-Gas HX with *Re*=4,138-11,191 and *Pr*= 9.8-18.9. By summing up the above studies, it is found that most experimental data fall in the deviation of 25% of traditional correlations, such as Gnielinski's correlation and Hansen's correlation. Besides, the CHTCs of Hitec in some noncircular passages, including the enhanced tube, annular passage, etc., have also been studied by Lu et al.[25-27], and corresponding correlations were obtained.

Recently, two studies also investigated the CHTCs of molten salt in the shell sides of the STHXs. He et al.[28] studied the CHTCs of Hitec outside a tube bundle with seven tubes. It is reported that the Nusselt numbers in the laminar region (*Re*=400-2300) is 3.5-5.0 times higher than those predicted by the traditional correlation. Du et al.[29] studied the CHTCs of Hitec in the shell side of a practical STHX with segmental baffles (STHE-SBs), where the flow is turbulent with *Re*=6142-9125 and *Pr*=19.43-22.33. The testing data was compared with a traditional correlation called Kern's correlation. It is found that this correlation is still appropriate to predict the CHTCs with a maximum deviation of 7.1%.

Based on the above review, on the one hand, it is seen that most studies focus on the CHTCs of molten salt in the tube side, but only one study has focused on the CHTCs in the shell side of a practical STHX. For understanding the heat transfer in the shell sides of the practical STHXs in CSP better, the CHTCs under realistic flow conditions are needed to be further investigated.

In this paper, a prototype rod baffle shell-and-tube heat exchanger (RB-STHX) was designed for CSP. RB-STHX proposed in 1970s [30] is a STHX that can eliminate the

harmful flow induced vibration in traditional STHE-SBs. This feature can also be helpful for the safe operation in CSP. For testing the CHTCs of molten salt in the shell side of the designed RB-STHX, a large-scale multipurpose molten salt testing facility was built. A ternary nitrate salt Hitec and a synthetic oil were used as the heat transfer fluids in the shell and tube sides, respectively. The experimental data was obtained and compared with two exiting correlations for the ordinary fluids. Based on the comparison, two new correlations were also developed.

2. RB-STHX and experimental facility

2.1 Prototype rod baffle shell-and-tube heat exchanger

A prototype rod baffle shell-and-tube heat exchanger (RB-STHX) made of 316L stainless steel was designed and constructed. The configuration is presented in Fig. 1, and three photos are shown in Fig. 2. The detailed geometric parameters are given in Table 1. The effective length of the RB-STHX is 2000 mm, and the inner diameter of the shell is 100 mm. A tube bundle with 21 tubes are installed in the shell using a square configuration as shown in Fig. 1 and Fig. 2. Eighteen rod baffles are placed along the flow direction in alternating orientation for disturbing the flow and supporting the tubes. Each baffle is made of a baffle ring welded with several parallel cylindrical rods as shown in Fig. 1 and Fig. 2. A thermal insulation layer of about 150 mm is used to cover the heat exchanger and reduce the heat loss in the experiment.

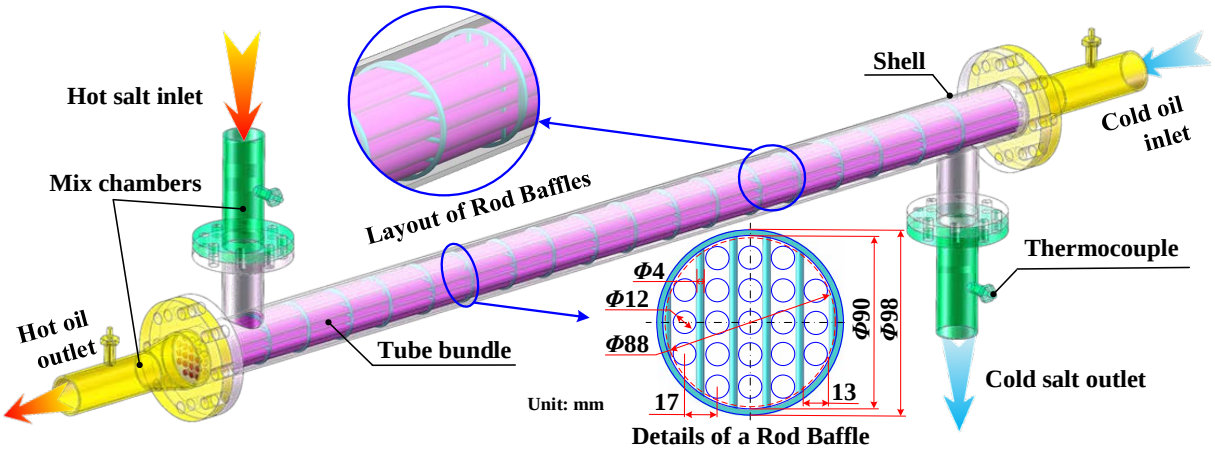

Fig. 1. Sketch of the rod baffle shell-and-tube HX showing the detailed layout of the baffle.

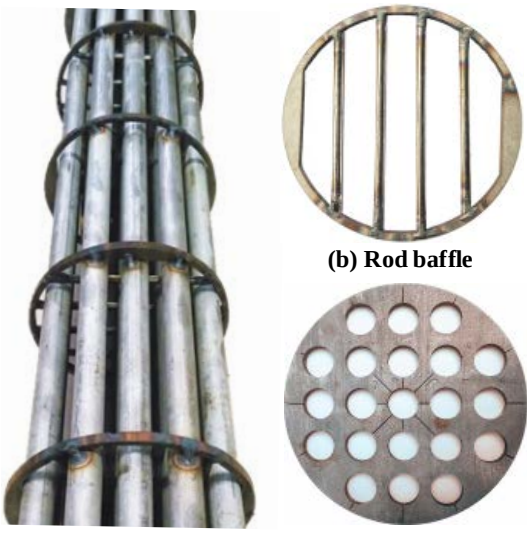

Fig. 2. Photos of the tube bundle, a rod baffle and an end plate.

Table 1 Detailed geometric parameters of the RB-STHX.

Parameters	Dimensions
Shell outer diameter	108 mm
Shell inner diameter D_s	100 mm
Shell-side inlet/outlet diameter	68 mm
Distance between head and shell-side inlet's axis	150 mm
Distance between head and shell-side outlet's axis	150 mm
Tube-side inlet/outlet diameter	68 mm
Tube arrangement	Square
Tube number n_t	21
Tube pitch	17 mm
Tube outer diameter d_o	12 mm
Tube inner diameter d_i	8 mm
Tube effective length L_t	2000 mm
Baffle number	18
Baffle distance from head	150 mm
Baffle pitch L_b	100 mm
Baffle thickness	4 mm
Rod diameter of baffle	4 mm
Diameter of the circumcircle of tube bundle D_o	88 mm
Outer diameter of baffle ring D_{bo}	98 mm
Inner diameter of baffle ring D_{bi}	90 mm

2.2 Large-scale multipurpose molten salt testing facility

The turbulent convective heat transfer performance of the molten salt in the shell side of the RB-STHX is tested in a large-scale multipurpose molten salt testing facility built in Key Laboratory of Thermo-Fluid Science and Engineering of Ministry of Education, China. A

photo of the facility is presented in Fig. 3.

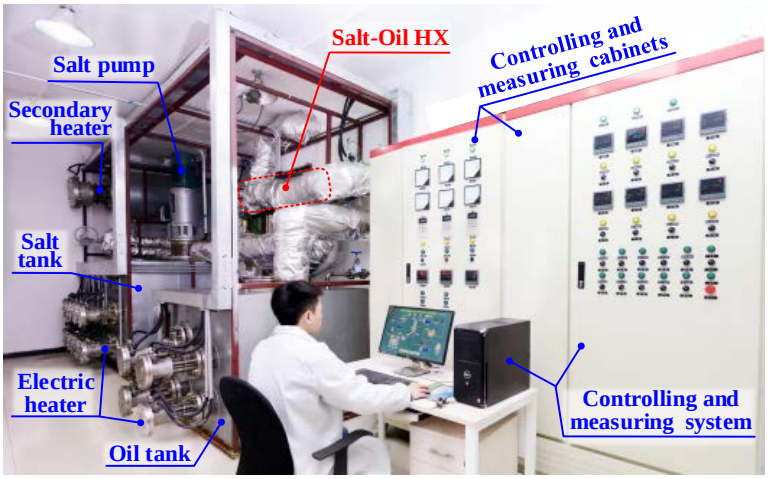

Fig. 3. Photo of the experimental facility.

The facility mainly consists of three loops including a salt loop, an oil loop, and a water loop. A detailed schematic of the facility is presented in Fig. 4, and a brief introduction of the loops and the experiment procedures are as follows.

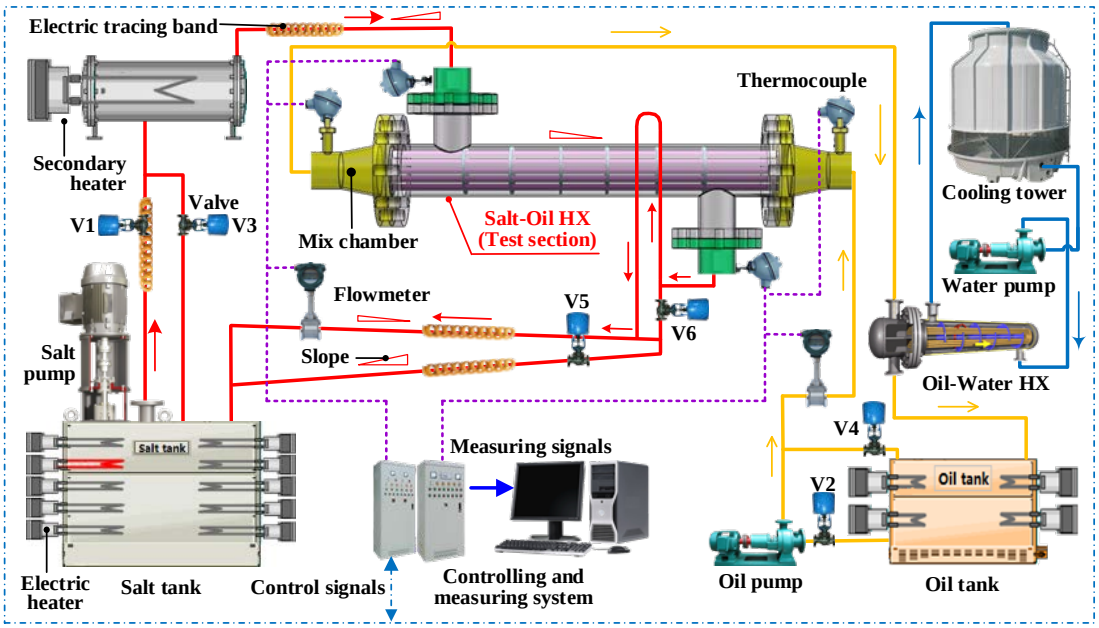

Fig. 4. Schematic of the experimental facility.

The salt loop mainly contains a salt tank with 6 tons of salt, a salt pump, a secondary heater, a flow meter and the shell side of the RB-STHX. The selected salt is a ternary nitrate salt (53 wt.% KNO_3, 40 wt.% $NaNO_2$, and 7 wt.% $NaNO_3$) which is well-known for the commercial name of Hitec. The limiting temperature and fusion point of Hitec are 535^{o}C and 142^{o}C, respectively. The maximum heating power in the salt tank is 122 kW. The design

volume flow rate of the salt pump is 25 $m^3 \cdot h^{-1}$. Small slopes of around 5^o have been designed for the pipes to help the salt to return to the tank as shown in Fig. 4. Electric tracing bands are employed to preheat the pipes for avoiding the solidification of the salt. At the outlet of the shell side, a U-shaped pipe has been designed for full filling the shell side during the experiment as shown in Fig. 4.

The oil loop mainly contains an oil tank with 2 tons of oil, an oil pump, a flow meter, the tube side of the RB-STHX, and the tube side of the oil-water HX. The selected oil is called YD-325 synthetic oil which has the limiting temperature of 325 ^{o}C. The maximum heating power in the oil tank is 60 kW. The design volume flow rate of the oil pump is 25 $m^3 \cdot h^{-1}$. In addition, the water loop mainly contains the shell-side of the oil-water exchanger, a water pump, and a cooling tower.

In the experiment, valves V1 and V2 in Fig. 4 are kept open, while valves V3-V6 are closed, and all pumps are turned on. The thermal power is firstly transferred from salt to oil in the RB-STHX. Then, the power is transferred from oil to water in the oil-water HX. Finally, the power is discharged into air through the cooling tower. The volume flow rates of salt and oil are measured by two vortex shedding flow meters with the relative uncertainty of 1.0%. The temperatures of salt and oil at the inlets and outlets of both shell and tube sides are measured using four K-type thermocouples with the uncertainty of 0.5^oC. Four mix chambers have been added to these nozzles for intensive mixing before the measurements as shown in Fig. 1. All thermocouples have also been calibrated using a standard platinum resistance thermometer with the uncertainty of 0.1^oC. The flow rate and temperature data are automatically recorded by a controlling and measuring system which is also used to control the heaters, pumps and valves.

The thermal physical properties of the Hitec and the YD-325 oil are calculated at the average temperature of the inlet and the outlet of corresponding side. Equations of the properties are presented in the Appendix. Fig. 5 shows variations of the Hitec's properties with the temperature. It is seen that μ_s, λ_s and ρ_s decrease with increasing temperature, while $c_{p,s}$ keeps constant. In addition, the constant conductivity of 16.3 $W \cdot (m \cdot K)^{-1}$ for the 316L

stainless steel is adopted.

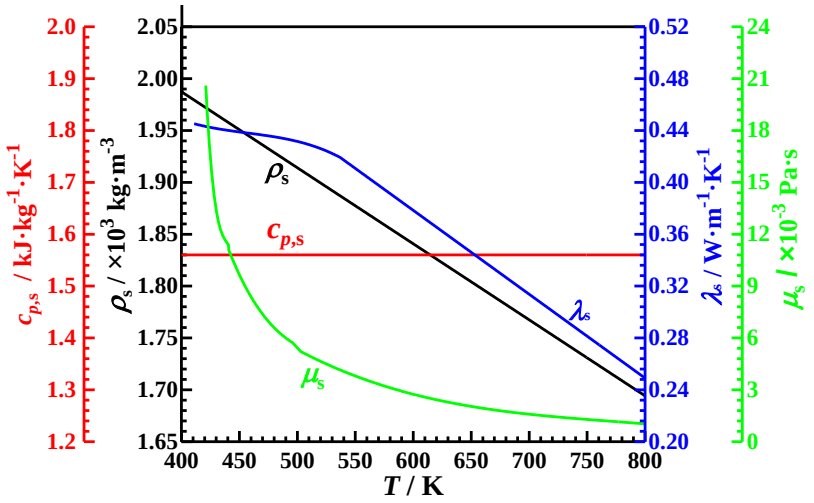

Fig. 5. Thermophysical properties of the ternary salt Hitec.

3. Data reduction

3.1 Heat transfer rate and energy balance

The heat transfer rates of the shell-side salt (Q_s) and tube-side oil (Q_t) in the RB-STHX are calculated using Eq.(1) and Eq.(2), respectively. The average value of Q_s and Q_t is regarded as the heat transfer rate of the exchanger (Q_{ave}) in Eq.(3). The thermal balance deviation (ε) of the exchanger is defined in Eq.(4).

$$Q_s = q_{V,s}\rho_s c_{p,s}\left(T_{s,in} - T_{s,out}\right) \tag{1}$$

$$Q_t = q_{V,t}\rho_t c_{p,t}\left(T_{t,out} - T_{t,in}\right) \tag{2}$$

$$Q_{ave} = \left(Q_s + Q_t\right)/2 \tag{3}$$

$$\varepsilon = \left|Q_s - Q_t\right| / Q_{ave} \times 100\% \tag{4}$$

where q_V represents the volume flow rate; c_p is specific heat; “t”,“s”, “in”, and “out” in the subscripts refer to the parameters of the tube side, shell side, inlet, and outlet, respectively.

3.2 Overall heat transfer coefficient

The overall heat transfer coefficient (K) between the shell side and tube side in the RB-STHX is defined in Eq.(5). The logarithmic mean temperature difference of the two sides (ΔT_m) is calculated by Eq.(6).

$$K = Q_{ave} / \left(A_o \Delta T_m\right) = Q_{ave} / \left(n_t \pi d_o L_t \cdot \Delta T_m\right) \tag{5}$$

$$\Delta T_{\mathrm{m}}=\frac{\left(T_{\mathrm{s,in}}-T_{\mathrm{t,out}}\right)-\left(T_{\mathrm{s,out}}-T_{\mathrm{t,in}}\right)}{\ln\left[\left(T_{\mathrm{s,in}}-T_{\mathrm{t,out}}\right)/\left(T_{\mathrm{s,out}}-T_{\mathrm{t,in}}\right)\right]} \tag{6}$$

where A_{o} is the heat transfer area based on the outer surfaces of the tubes.

3.3 Tube-side heat transfer coefficient

The tube-side convection heat transfer coefficient (h_{t}) is calculated by Gnielinski's equation in Eq.(8), where the characteristic dimension is the tube inner diameter. The friction factor (f) is calculated using Filonenko's equation in Eq.(9) [31].

$$h_{\mathrm{t}}=Nu_{\mathrm{t}}\lambda_{\mathrm{t}}/d_{\mathrm{i}} \tag{7}$$

$$Nu_{\mathrm{t}}=\frac{(f/8)\left(Re_{\mathrm{t}}-1000\right)Pr_{\mathrm{t}}}{1+12.7\cdot(f/8)^{0.5}\cdot\left(Pr_{\mathrm{t}}^{2/3}-1\right)}\left[1+\left(\frac{d_{\mathrm{i}}}{L_{\mathrm{t}}}\right)^{2/3}\right]\cdot\left(\frac{Pr_{\mathrm{t}}}{Pr_{\mathrm{w}}}\right)^{0.11} \tag{8}$$

$$f=\left(1.82\lg Re_{\mathrm{t}}-1.64\right)^{-2} \tag{9}$$

$$Re_{\mathrm{t}}=\left(\rho_{\mathrm{t}}u_{\mathrm{t}}d_{\mathrm{i}}\right)/\mu_{\mathrm{t}} \tag{10}$$

where $Pr_{\mathrm{t}}/Pr_{\mathrm{w}}=0.05\sim20, Re_{\mathrm{t}}=2300\sim10^{6}, Pr_{\mathrm{t}}=0.6\sim10^{5}$.

3.4 Shell-side heat transfer coefficient and Nusselt number

The shell-side convection heat transfer coefficient (h_{s}) is calculated by Eq.(11).

$$h_{\mathrm{s}}=\frac{1}{\frac{1}{K}-\frac{1}{h_{\mathrm{t}}}\frac{d_{\mathrm{o}}}{d_{\mathrm{i}}}-\frac{d_{\mathrm{o}}}{2\lambda_{\mathrm{w}}}\ln\frac{d_{\mathrm{o}}}{d_{\mathrm{i}}}} \tag{11}$$

where λ_{w} is the heat conductivity of the tube wall.

Nusselt number of shell side is calculated by Eq.(12). The Reynolds number of the shell side is expressed in Eq. (13).

$$Nu_{\mathrm{s}}=h_{\mathrm{s}}D_{\mathrm{h}}/\lambda_{\mathrm{s}} \tag{12}$$

$$Re_{\mathrm{s}}=\rho_{\mathrm{s}}u_{\mathrm{s}}D_{\mathrm{h}}/\mu_{\mathrm{s}} \tag{13}$$

$$u_{\mathrm{s}}=4q_{V,\mathrm{s}}/\left[\pi\left(D_{\mathrm{s}}^{2}-n_{\mathrm{t}}d_{\mathrm{o}}^{2}\right)\right] \tag{14}$$

$$D_{\mathrm{h}}=\left(D_{\mathrm{s}}^{2}-n_{\mathrm{t}}\cdot d_{\mathrm{o}}^{2}\right)/\left(D_{\mathrm{s}}+n_{\mathrm{t}}\cdot d_{\mathrm{o}}\right) \tag{15}$$

where D_{h} and u_{s} are the hydraulic diameter and velocity of the shell side, respectively.

3.5 Uncertainty analysis

The uncertainties of the experimental data were evaluated using the method presented in Refs.[32, 33]. In this method, it assumes that a desired variable (R) can be expressed as a function of n independent measured parameters (x_1, x_2, …, x_n). So, the relative uncertainty ($\delta R/R$) of R can be calculated by Eq.(17). Table 2 shows the uncertainties of the measured and calculated parameters. It is seen that the relative uncertainties of Q_{ave}, K, Re_s and Nu_s are within 8.3%, 8.3%,1.7% and 8.4%, respectively.

$$R = f\left(x_1, x_1, \cdots, x_n\right) \tag{16}$$

$$\frac{\delta R}{R} = \left[\sum_{i=1}^{n}\left(\frac{\partial f}{x_i}\delta x_i\right)^2\right]^{0.5} \Big/ R \tag{17}$$

where δx_i is the uncertainty of variable x_i.

4. Results and discussion

The turbulent convective heat transfer characteristics of the molten salt in the shell side of the RB-STHX was experimentally studied using the previous described approach. The detailed experimental conditions are given in Table 2. During the experiment, the average temperatures of salt and oil are in the ranges of 212.7-279.6^{o}C and 95.5-154.0^{o}C, respectively. The volume flow rates of salt and oil are in the ranges of 8.42-24.99 $m^3 \cdot h^{-1}$ and 19.10-19.51$m^3 \cdot h^{-1}$, respectively.

Table 2 The measured and calculated parameters showing their uncertainties.

Items	Parameters	Range	Absolute or relative uncertainty
Measured parameters of shell side	$q_{V,s}$ / $m^3 \cdot h^{-1}$	8.42-24.99	±1%
	$T_{s,in}$ / ^{o}C	221.6-290.4	±0.5^{o}C
	$T_{s,out}$ / ^{o}C	203.8-268.9	±0.5^{o}C
Measured parameters of tube side	$q_{V,t}$ / $m^3 \cdot h^{-1}$	19.10-19.51	±1%
	$T_{t,in}$ / ^{o}C	83.4-146.4	±0.5^{o}C
	$T_{t,out}$ / ^{o}C	107.5-161.6	±0.5^{o}C
Desired parameters	Q_{ave} / kW	117-364	8.3%
	K / $W \cdot m^{-2} \cdot {}^{o}C^{-1}$	903-1,559	8.3%
	Re_s	2,697-12,517	1.7%
	Nu_s	71-190	8.4%

4.1 Thermal balance check and experimental results

The thermal balance between the shell side and tube side was checked in the experiment. The check results at different *Re* are shown in Fig. 6. It can be seen that the thermal balance deviations for the obtained experimental data are within 7%. These results indicate that the present experimental facility and the testing approach are dependable and suitable.

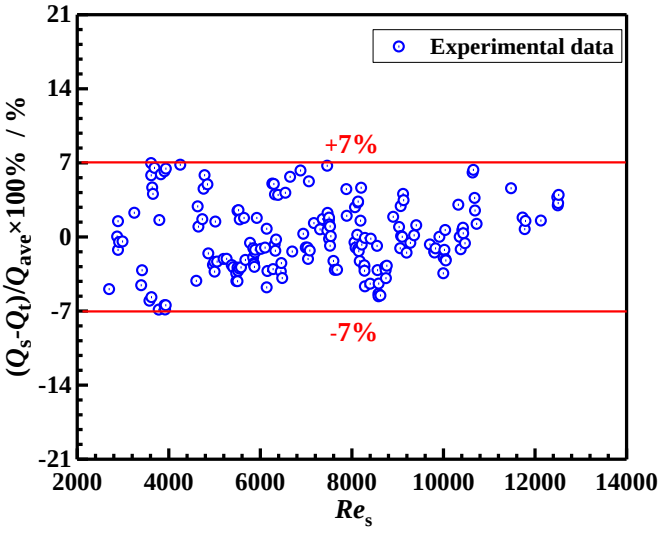

Fig. 6. Thermal balance check of the experiment.

The testing data were reduced, and the experimental results of the Nusselt number (Nu_s) at different Reynolds numbers (Re_s) are shown in Fig. 7. It is seen that Nu_s increases with the increase in Re_s, which is similar with those of ordinary fluids. This is due to a well-known reason that the larger the *Re* is, the more intensive the turbulence becomes. In the experiment, the flow is turbulent, and the Re_s is in the range of 2,697-12,517. The Nu_s ranges between 71 and 190. The Pr_s varies from 14.2 to 23.3. The average heat transfer rate ranges from 117 kW to 364 kW. Because the temperature difference between the salt and oil sides is quite large, the average temperature difference of 50.3-105.2^{o}C between the salt and the tube wall occurs in the test. As a result, the (μ_f/μ_w) of 0.35-0.60 can also be found.

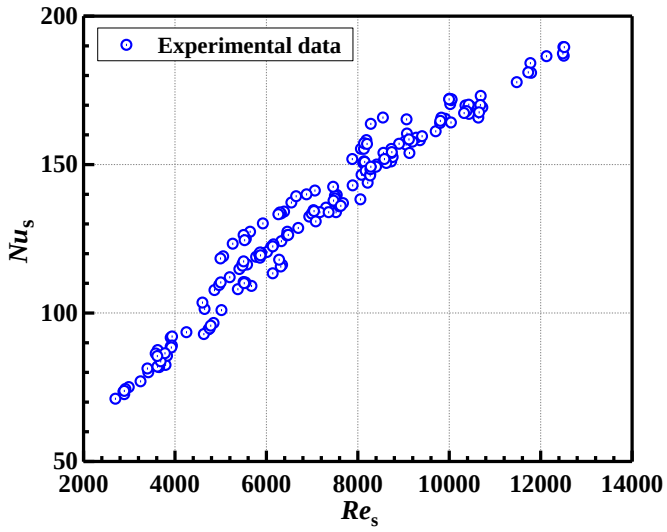

Fig. 7. Experimental result of the salt in shell side.

4.2 Comparison of experimental data and exiting correlations

For describing the turbulent convective heat transfer of single-phase fluids in a heat exchanger (HX) in a general way, the Nu_s is usually expressed as a power function of Re_s and Pr_s as shown in Eq.(18), where C_1 is a factor defined by the geometric parameters of the HX. m and n are constants. m is usually around 0.8 for turbulent flow, and n is usually around 0.4 or 1/3. Moreover, in order to consider the temperature difference between the fluid and the wall, another term (C_2) which is usually a function of the viscosity or the Prandtl number is also added.

$$Nu_s = C_1 \cdot Re_s^m Pr_s^n \cdot C_2 \tag{18}$$

For the RB-STHX, some correlations which are usually obtained using oil or water as the heat transfer fluid can be found in the literature. The current experimental data are compared with two of the typical existing correlations.

The first one is a correlation provided by the Phillips petroleum company in Ref.[30] as shown in Eqs.(19) and (20) (hereafter Correlation A). In this equation, m of 0.8 and n of 0.4 are adopted, and C_2 is a function of the viscosity. For current tested RB-STHX, C_1 in Eq.(19) equals to 0.0352.

$$Nu_s = C_1 Re_s^{0.8} Pr_s^{0.4} \left(\frac{\mu_s}{\mu_w} \right)^{0.14} \tag{19}$$

$$\begin{cases} C_1 = C \cdot \xi \\ C = \left(0.042 - 0.0417\lambda\right) + \left(0.023 - 0.0117\lambda\right) e^{-0.00496 L_b} \\ \lambda = \left[\dfrac{\left(D_s^2 - D_o^2\right) - \left(D_{bo}^2 - D_{bi}^2\right)}{D_s^2 - n_t d_o^2} + 0.1 \right]^{0.5} \\ \xi = 0.96 + 0.2437 e^{-0.01614\left(L_t / D_{bo} - 1\right)^2} \end{cases} \tag{20}$$

Fig. 8 shows the comparison of current experimental data with Correlation A. It can be observed that most experimental data are larger than the values predicted by Correlation A. The deviations between the experimental data and the predicted values range from -3% to +20%. The average deviations of approximately 10% can be found at the same Reynolds numbers.

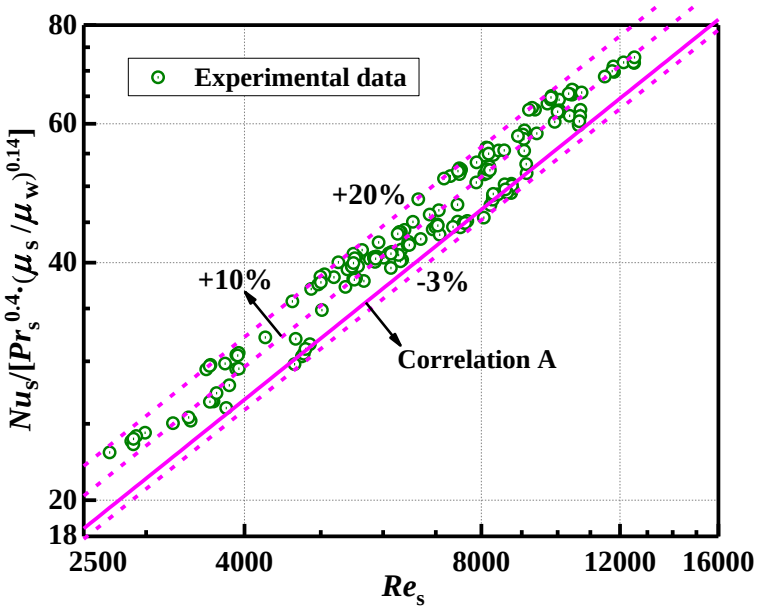

Fig. 8. Comparison of the experimental data with Correlation A.

The second correlation is an equation described in Ref.[34] as shown in Eq.(21) (hereafter Correlation B). In this correlation, m of 0.815 and n of 1/3 are adopted, and C_2 is a function of the viscosity. For the tested RB-STHX, C_1 in Eq.(21) equals to 0.0361.

$$Nu_s = C_1 \cdot Re_s^{0.815} Pr_s^{1/3} \cdot \left(\frac{\mu_s}{\mu_w} \right)^{0.14}, C_1 = 0.0589 \left(\frac{L_b}{D_e} \right)^{-0.303} \tag{21}$$

Fig. 9 shows the comparison of current experimental data with Correlation B. It can be observed that the deviations between the experimental results and the predicted values are in the range of +1~+26%. Furthermore, most experimental data are larger than the values predicted by Correlation B. The average deviations of around +14% can be found at the identical Reynolds numbers.

To sum up, comparing with the experimental data, the average underestimates for correlations A and B are 9.1% and 12.3%, respectively. Similar phenomenon has also been reported in the heat transfer of molten salt in the circular tube. For example, it is reported in Ref.[22] by Chen et al. that the Sieder-Tate correlation and the Hausen correlation underestimate about 8% and 10% compared with the experimental results, respectively.

Therefore, in order to have a better understanding of the heat transfer characteristics in the shell side of RB-STHX, a correlation which can get better predictions of the experimental data would be welcomed by the practitioners in CSP.

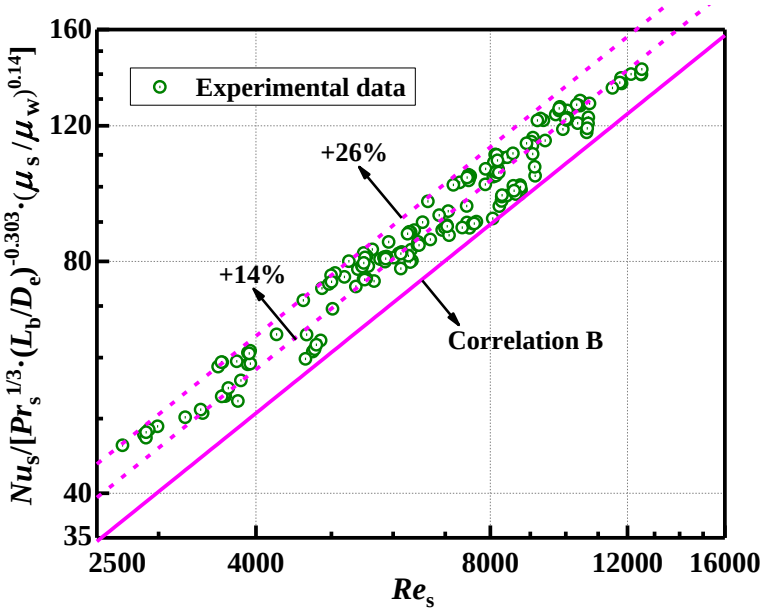

Fig. 9. Comparison of the experimental data with Correlation B.

4.3 Modified heat transfer correlations

In this section, the data of Nusselt number obtained from the experiment for the molten salt in the shell side are fitted into two heat transfer correlations, which are in the forms of Correlation A and Correlation B, respectively.

The first modified correlation fitted in the form of Correlation A is given in Eq.(22). It

has the same C_1, n and viscosity term as those in Correlation A. However, a modified m of 0.775 and a new constant term φ of 1.375 are obtained by fitting the data. The goodness of the fit is 0.959. For current RB-STHX, the correlation can be rewritten as Eq.(23).

$$Nu_s = \varphi \cdot C_1 Re_s^{0.775} Pr_s^{0.4} \left(\frac{\mu_s}{\mu_w} \right)^{0.14}, \ \varphi = 1.375 \tag{22}$$

$$Nu_s = 0.0484 \cdot Re_s^{0.775} Pr_s^{0.4} \left(\frac{\mu_s}{\mu_w} \right)^{0.14} \tag{23}$$

where C_1 is the same as that in Eq.(20). The examined ranges of key parameters are as follows. Re_s=2,697-12,517, Pr_s=14.2-23.3, and $(\mu_s/\mu_w)^{0.14}$=0.86-0.93.

Fig. 10 presents the fitted correlation along with the experimental data and Correlation A. It is seen that the current experimental results are in good agreement with the fitted correlation with an average deviation of ±4.6% and a maximum deviation of ±11.5%. Moreover, an average deviation of -9.3% and a maximum deviation of -11.3% between Correlation A and the modified correlation can also be observed.

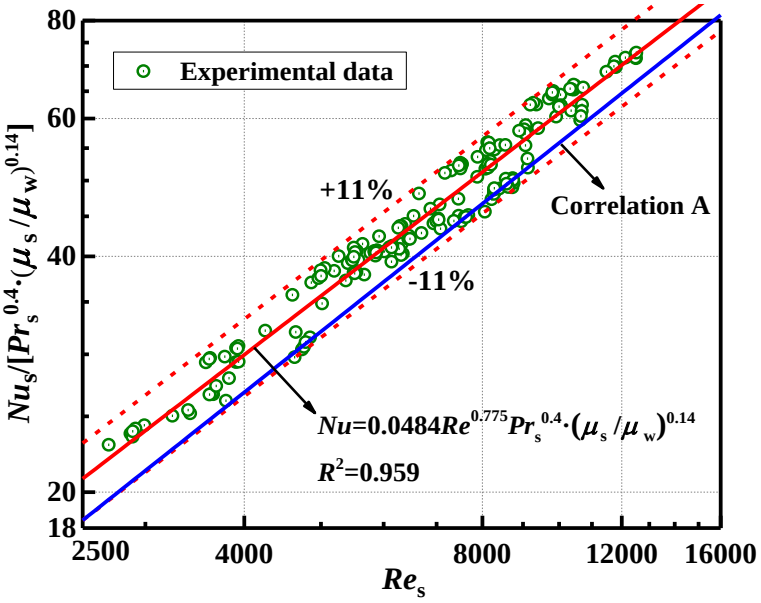

Fig. 10. Fitting correlation of the experimental data and Correlation A.

The second modified correlation fitted in the form of Correlation B is given in Eq.(24). It has the same n and viscosity term as those in Correlation B. However, a modified m of 0.756 and a revised C_1 is obtained by fitting the data. The goodness of the fit of 0.962 is achieved. For current RB-STHX, the modified correlation can be rewritten as Eq.(25).

$$Nu_s = C_1 Re_s^{0.756} Pr_s^{1/3} \left(\frac{\mu_s}{\mu_w}\right)^{0.14}, C_1 = 0.1133 \left(\frac{L_b}{D_e}\right)^{-0.303} \quad (24)$$

$$Nu_s = 0.0694 \cdot Re_s^{0.756} Pr_s^{1/3} \left(\frac{\mu_s}{\mu_w}\right)^{0.14} \quad (25)$$

where the examined ranges of key parameters are as follows. Re_s=2,697-12,517, Pr_s=14.2-23.3, and $(\mu_s/\mu_w)^{0.14}$=0.86-0.93.

Fig. 11 shows the second modified correlation, the experimental data, and Correlation B. It can be observed that the current experimental results agree with the fitted correlation well with an average deviation of ±4.4% and a maximum deviation of ±10.7%. In addition, an average deviation of -12.5% between the modified correlation and Correlation A is observed, and a maximum deviation of -17.5% is also found.

The above results indicate that the two modified correlations can predict the heat transfer of the ternary salt Hitec in the shell side of current RB-STHX more accurately than the two exiting correlations. As a result, we think the modified correlations can be applied in the heat transfer calculation of the RB-STHX in CSP.

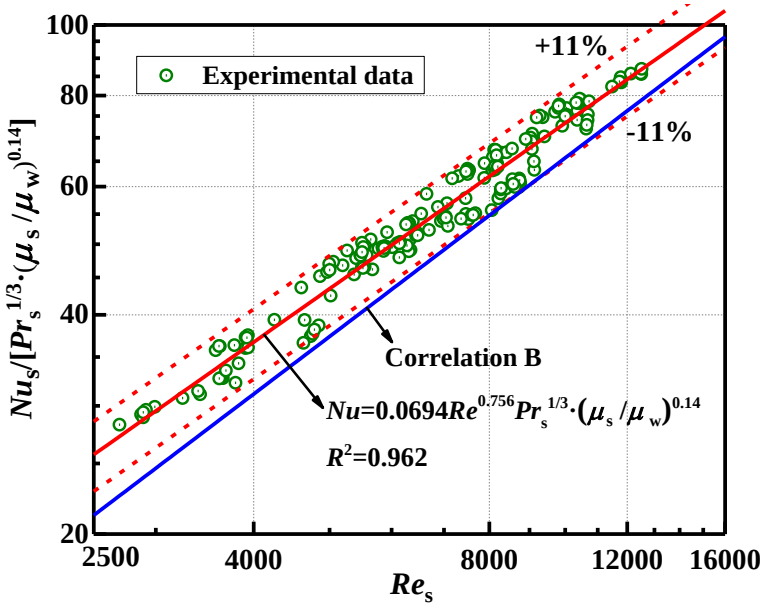

Fig. 11. Fitting correlation of the experimental data and Correlation B.

5. Conclusions

In this paper, turbulent convective heat transfer characteristics of a ternary salt Hitec in

the shell side of a prototype rod baffle shell-and-tube heat exchanger (RB-STHX) for the CSP was experimentally studied. The conclusions are as follow:

(1) Experimental data was obtained in the salt temperature range of 212.7-279.6^{o}C. The flow is turbulent with the volume flow rate of 8.42-24.99 $m^3 \cdot h^{-1}$, and the corresponding Re_s ranges from 2,697 to 12,517.

(2) The experimental data was compared with two exiting correlations obtained using ordinary fluids. The comparison indicates that the turbulent convective heat transfer characteristics of Hitec in the shell side of the RB-STHX are close to the exiting correlations. Nevertheless, the predicted Nusselt numbers of the exiting correlations could not describe the heat transfer characteristics accurately with an average underestimate of 9.1-12.3%.

(3) Based on the comparison, two modified heat transfer correlations for Hitec are developed, and they have satisfactory agreements with the experimental data. The first correlation is $Nu_s = 1.375 \cdot C_1 \cdot Re_s^{0.775} Pr_s^{0.4} \left(\mu_s/\mu_w\right)^{0.14}$, where C_1 is a parameter defined in Eq.(20). The second correlation is $Nu_s = 0.1133 \left(L_b/D_e\right)^{-0.303} \cdot Re_s^{0.756} Pr_s^{1/3} \left(\mu_s/\mu_w\right)^{0.14}$. The examined ranges of key parameters are as follows. Re_s=2,697-12,517, Pr_s=14.2-23.3, and $(\mu_s/\mu_w)^{0.14}$=0.86-0.93.

These results will offer the reliable data and helpful guidance for the design and operation of realistic molten salt RB-STHXs in the CSP systems.

Acknowledgements

The study is supported by the funding for Key Project of National Natural Science Foundation of China (No.51436007).

Appendix

The properties of the ternary salt (Hitec) are described by equations A(1)-A(4).

$$\rho_s = -0.733T + 2280.22,\ 420\text{K} \le T \le 800\text{K} \quad \text{A(1)}$$

$$c_{p,s} = 1560,\ 420\text{K} \le T \le 800\text{K} \quad \text{A(2)}$$

$$k_s = \begin{cases} -1.863\times10^{-8}T^3 + 2.551\times10^{-5}T^2 \\ -0.01176T + 2.2627 \quad ,\ 420\text{K} \le T < 536\text{K} \\ -6.47\times10^{-4}T + 0.7663,\ 536\text{K} < T \le 800\text{K} \end{cases} \quad \text{A(3)}$$

$$\mu_s=\begin{cases}-1.742173\times10^{-6}T^3+2.27615\times10^{-3}T^2\\-0.99143T+143.9826 \quad ,420\text{K}\le T<440\text{K}\\-7.2058\times10^{-9}T^3+1.08225\times10^{-5}T^2\\-5.4754\times10^{-3}T+0.93845,440\text{K}\le T<500\text{K}\\8.507\times10^{-13}T^4-2.4331\times10^{-9}T^3+2.6275\times10^{-6}T^2\\-1.2768\times10^{-3}T+0.23816\ ,500\text{K}\le T\le800\text{K}\end{cases} \quad \text{A(4)}$$

The properties of YD-325 synthetic oil are described by equations A(5)-A(8).

$$\rho_t=-0.6311T+1199.13,\ 300\text{K}\le T\le573\text{K} \quad \text{A(5)}$$

$$c_{p,t}=3.40T+776.0,\ 300\text{K}\le T\le573\text{K} \quad \text{A(6)}$$

$$k_t=-6.68\times10^{-5}T+0.1416,\ 300\text{K}<T\le573\text{K} \quad \text{A(7)}$$

$$\mu_t=\begin{cases}-4.066\times10^{-9}T^3+5.2746\times10^{-6}T^2\\-2.283\times10^{-3}T+0.33065,\ 323\text{K}<T\le423\text{K}\\-4.413\times10^{-10}T^3+6.735\times10^{-7}T^2\\-3.452\times10^{-4}T+0.05989,\ 423\text{K}<T\le523\text{K}\end{cases} \quad \text{A(8)}$$

Nomenclature

A_o	area of the outer surfaces of tubes (m^2)
$c_{p,s}$ / $c_{p,t}$	specific heat of salt / oil ($J\cdot kg^{-1}\cdot K^{-1}$)
CHTCs	convective heat transfer characteristics
D_h	hydraulic diameter of the shell side (m, mm)
D_s	shell inner diameter (m, mm)
D_o	diameter of the circumcircle of tube bundle (m, mm)
D_{bo}	outer diameter of baffle ring (m, mm)
D_{bi}	inner diameter of baffle ring (m, mm)
d_o	Tube outer diameter (m, mm)
d_i	Tube inner diameter (m, mm)
f	friction factor
h_s / h_t	heat transfer coefficient of shell / tube side ($W\cdot m^{-2}\cdot K^{-1}$)
K	overall heat transfer coefficient ($W\cdot m^{-2}\cdot K^{-1}$)
L_t	tube effective length (m, mm)
L_b	baffle pitch (m, mm)
Nu_s / Nu_t	Nusselt number of shell / tube side
n_t	tube number
Pr_s / Pr_t	Prandtl number of shell / tube side
Pr_w	Prandtl number using wall temperature as the qualitative temperature

Q_s / Q_t	heat transfer rate of shell / tube side (kW)
Q_{ave}	heat transfer rate of the heat exchanger (kW)
$q_{V,s}$ / $q_{V,t}$	volume flow rate of shell / tube side ($m^3 \cdot h^{-1}$)
Re_s / Re_t	Reynolds number of shell / tube side
RB-STHX	rod baffle shell-and-tube heat exchanger
STHX	shell-and-tube heat exchanger
T	temperature (K, ^oC)
u_s / u_t	velocity of the shell / tube side ($m \cdot s^{-1}$)

Greek symbols

ΔT_m	logarithmic mean temp. difference of two sides (K)
ε	thermal balance deviation (%)
λ_w	heat conductivity of the tube wall ($W \cdot m^{-1} \cdot K^{-1}$)
λ_s / λ_t	heat conductivity of salt / oil ($W \cdot m^{-1} \cdot K^{-1}$)
μ_s / μ_t	dynamic viscosity of salt / oil (Pa·s)

Subscripts

s, t, in, out	parameters of tube side / shell side / inlet / outlet
ave	average value

Reference

[1] Spracklen DV. Global warming: China's contribution to climate change. Nature. 2016;531:310-2.

[2] Li MJ, Song CX, Tao WQ. A hybrid model for explaining the short-term dynamics of energy efficiency of China's thermal power plants. Appl Energ. 2016;169:738-47.

[3] Li MJ, Tao WQ. Review of methodologies and polices for evaluation of energy efficiency in high energy-consuming industry. Appl Energ. 2017;187:203-15.

[4] Li MJ, He YL, Tao WQ. Modeling a hybrid methodology for evaluating and forecasting regional energy efficiency in China. Appl Energ. 2015:DOI:10.1016/j.apenergy.2015.11.082.

[5] He YL, Wang K, Du BC, Qiu Y, Liang Q. Non-uniform characteristics of solar flux distribution in the concentrating solar power systems and its corresponding solutions: A review. Chin Sci Bull. 2016;61:3208-37.

[6] Lewis NS. Research opportunities to advance solar energy utilization. Science. 2016;351:aad1920.

[7] Ma Z, Yang WW, Yuan F, Jin B, He YL. Investigation on the thermal performance of a high-temperature latent heat storage system. Appl Therm Eng. 2017;122:579-92.

[8] Wu M, Xu C, He Y. Cyclic behaviors of the molten-salt packed-bed thermal storage system filled with cascaded phase change material capsules. Appl Therm Eng. 2016;93:1061-73.

[9] Kuravi S, Trahan J, Goswami DY, Rahman MM, Stefanakos EK. Thermal energy storage technologies and systems for concentrating solar power plants. Prog Energ Combust. 2013;39:285-319.

[10] Qiu Y, He YL, Cheng ZD, Wang K. Study on optical and thermal performance of a linear Fresnel solar reflector using molten salt as HTF with MCRT and FVM methods. Appl Energ. 2015;146:162-73.

[11] Qiu Y, He YL, Wu M, Zheng ZJ. A comprehensive model for optical and thermal characterization of a linear Fresnel solar reflector with a trapezoidal cavity receiver. Renew Energ. 2016;97:129-44.

[12] He YL, Xiao J, Cheng ZD, Tao YB. A MCRT and FVM coupled simulation method for energy conversion process in parabolic trough solar collector. Renew Energ. 2011;36:976-85.

[13] Qiu Y, Li MJ, He YL, Tao WQ. Thermal performance analysis of a parabolic trough solar collector using supercritical CO2 as heat transfer fluid under non-uniform solar flux. Appl Therm Eng. 2017;115:1255-65.

[14] Qiu Y, He YL, Li PW, Du BC. A comprehensive model for analysis of real-time optical performance of a solar power tower with a multi-tube cavity receiver. Appl Energ. 2017;185:589-603.

[15] Grele MD, Gedeon L. Forced-convection heat-transfer characteristics of molten Flinak flowing in an inconel X system. Washington: National Advisory Committee for Aeronautics; 1954.

[16] Hoffman HW, Lones J. Fused salt heat transfer. Part II. Forced convection heat transfer in circular tubes containing NaF-KF-LiF eutectic. Oak Ridge: Oak Ridge National Laboratory; 1955.

[17] Hoffman HW, Cohen SI. Fused salt heat transfer: Part III: Forced-convection heat transfer in circular tubes containing the salt mixture NaNO2-NaNO3-KNO3. Oak Ridge: Oak Ridge National Laboratory; 1960.

[18] Cooke JW, Cox BW. Forced-convection heat transfer measurements with a molten fluoride salt mixture flowing in a smooth tube. Oak Ridge: Oak Ridge National Laboratory; 1973.

[19] Silverman MD, Huntley WR, Robertson HE. Heat transfer measurements in a forced convection loop with two molten-fluoride salts LiF-BeF2-ThF2-UF4 and eutectic NaBF4-NaF. Oak Ridge: Oak Ridge National Laboratory; 1976.

[20] Liu B, Wu YT, Ma CF, Ye M, Guo H. Turbulent convective heat transfer with molten salt in a circular pipe. Int Commun Heat Mass. 2009;36:912-6.

[21] Wu YT, Liu B, Ma CF, Guo H. Convective heat transfer in the laminar-turbulent transition region with molten salt in a circular tube. Exp Therm Fluid Sci. 2009;33:1128-32.

[22] Chen YS, Wang Y, Zhang JH, Yuan XF, Tian J, Tang ZF, et al. Convective heat transfer characteristics in the turbulent region of molten salt in concentric tube. Appl Therm Eng. 2016;98:213-9.

[23] He YL, Zheng ZJ, Du BC, Wang K, Qiu Y. Experimental investigation on turbulent heat transfer characteristics of molten salt in a shell-and-tube heat exchanger. Appl Therm Eng. 2016;108:1206-13.

[24] Qian J, Kong Q, Zhang H, Huang W, Li W. Performance of a gas cooled molten salt heat exchanger. Appl Therm Eng. 2016;108:1429-35.

[25] Lu J, He S, Liang J, Ding J, Yang J. Convective heat transfer in the laminar–turbulent transition region of molten salt in annular passage. Exp Therm Fluid Sci. 2013;51:71-6.

[26] Lu J, Sheng X, Ding J, Yang J. Transition and turbulent convective heat transfer of molten salt in spirally grooved tube. Exp Therm Fluid Sci. 2013;47:180-5.

[27] Lu J, He S, Ding J, Yang J, Liang J. Convective heat transfer of high temperature molten salt in a vertical annular duct with cooled wall. Appl Therm Eng. 2014;73:1519-24.

[28] He S, Lu J, Ding J, Yu T, Yuan Y. Convective heat transfer of molten salt outside the tube bundle of heat exchanger. Exp Therm Fluid Sci. 2014;59:9-14.

[29] Du BC, He YL, Wang K, Zhu HH. Convective heat transfer of molten salt in the shell-and-tube heat exchanger with segmental baffles. Int J Heat Mass Tran. 2017;113:456-65.

[30] Gentry CC. Rodbaffle heat exchanger technology. Chem Eng Prog. 1990;86:48-57.

[31] Yang SM, Tao WQ. Heat transfer. 4th ed. Beijing: High Education Press; 2006.

[32] Kline SJ, Mcclintock FA. Describing uncertainties in single-sample experiments. Mech Eng. 1953;75:3-8.

[33] Moffat RJ. Describing the uncertainties in experimental results. Exp Therm Fluid Sci. 1988;1:3-17.

[34] Dong QW, Wang YQ, Liu MS. Numerical and experimental investigation of shellside characteristics for RODbaffle heat exchanger. Appl Therm Eng. 2008;28:651-60.